Analysis and Design of Three-Stage Concatenated Color-Shift Keying

Junyi Jiang, Rong Zhang, *Member, IEEE*, and Lajos Hanzo, *Fellow, IEEE*

***Abstract*—Visible light communication (VLC) relies on abundant unlicensed bandwidth resources. As an attractive high-data-rate modulation scheme designed for VLC, color shift keying (CSK)-assisted modulation is analyzed. We commence our study from an uncoded M-CSK scheme relying on the joint maximum-likelihood (ML) hard detection (HD) of three colors when communicating over an AWGN channel, where both empirical and analytical results are provided. We invoke extrinsic information transfer (EXIT) charts for designing a Maximum *a posteriori* probability (MAP)-based soft detection (SD)-aided iterative receiver jointly detecting the three colors. Based on the EXIT characteristics of M-CSK, we design different signal labeling strategies for diverse color constellations and detection schemes, which are capable of achieving a substantially improved bit-error-rate (BER) performance. Thus, given fixed transmission power, a CSK system using our proposed signal labeling is capable of increasing the reliable data transmission distance by about 30%.**

***Index Terms*—Color constellation, color shift keying (CSK), extrinsic information transfer (EXIT) chart, iterative receiver, near capacity, signal labeling.**

I. Introduction

To minimize the risk of the impending capacity crunch imposed by the exponentially increased mobile data explosion, heterogeneous networks (HetNets) composed of multiple radio access technologies (RATs), relying on diverse cellular architectures and adaptive transmission modes, have been recognized as one of the most promising solutions. Hence, the fifth-generation (5G) wireless system is expected to rely on the HetNet philosophy [1], [2]. Among others, millimeter-wave communications (MWC) [3] and visible light communications (VLC) [4]–[9] constitute a pair of important complementary access technologies in addition to the development of traditional RAT along the Long-Term Evolution "avenue" [10]. In particular, VLC has attracted substantial research attention across both the academic and industrial communities since it provides abundant license-free bandwidth, which is free from microwave pollutions, while supporting the dual purpose of both communications and illumination.

As an appealing optical wireless communication technology, both high-brightness white and colored light-emitting diodes (LEDs) [5], [12]–[14] may be used for conveying information. As a benefit of their long life expectancy, high lighting efficiency, and small size, LED devices are routinely used by car manufacturers in both headlights and taillights. This provides a valuable opportunity for exploiting VLC as a part of the road infrastructure for conveying the teletraffic with the aid of traffic lights, streetlights, and for vehicle-to-vehicle communications using the headlights and taillights. The development of VLC schemes has led to the definition of an IEEE standard [5], [16], which is known as 802.15.7, where the so-called color shift keying (CSK) is used for high-data-rate transmission. To elaborate a little further, Drost and Sadler proposed a CSK constellation design using the so-called Billiards algorithm of [19] and expanded their research to an arbitrary number of LEDs in [20]; as a further development, Monterio and Hranilovic proposed another design by invoking the interior point method of [21] and [22], where optimized color constellations were proposed. Furthermore, Singh *et al.* [23] conceived a novel QuadCSK arrangement by invoking four source lights. Finally, a multiuser CSK scheme was presented by Luna-Rivera *et al.* in [24]. Nonetheless, at the time of writing, there is a paucity of research on iterative CSK transceiver design; hence, in this paper, we analyze the performance of the M-CSK system's color constellation and design its bit-to-symbol mapping. Our contributions are thus twofold.

- We conceive the maximum *a posteriori* probability (MAP)-based soft detection (SD) of CSK and characterize its *extrinsic* mutual information improvement achieved by our iterative receiver with the aid of extrinsic information transfer (EXIT) charts [25]–[27].
- We characterize the performance limitations of the IEEE standard's constellation labeling, and we circumvent them by designing improved signal labeling strategies with the aid of EXIT charts [28]. As a result, we demonstrate that the power gain attained by this signal labeling improves the achievable transmission distance and/or enhances the link's reliability in vehicular VLC applications.

The remainder of this paper is organized as follows. In Section II, we briefly introduce the CSK modulation philosophy, including its color coding and intensity conversion techniques. Both ML-based hard detection (HD) and MAP-based SD are characterized. In Section III, we focus our attention

Manuscript received July 7, 2014; revised November 3, 2014; accepted December 13, 2014. This work was supported in part by the Research Council U.K. under the auspices of the India–U.K. Advanced Technology Centre and of the European Union Concerto Project and in part by the European Research Council under an Advanced Fellow Grant. The review of this paper was coordinated by Prof. Y. Su.

J. Jiang and R. Zhang are with the Wireless Group, School of Electronics and Computer Science, SO17 1BJ Southampton, U.K.

L. Hanzo is with the School of Electronics and Computer Science, SO17 1BJ Southampton, U.K., and also with Tsinghua University Beijing 100084, China.

Digital Object Identifier 10.1109/TVT.2014.2382875

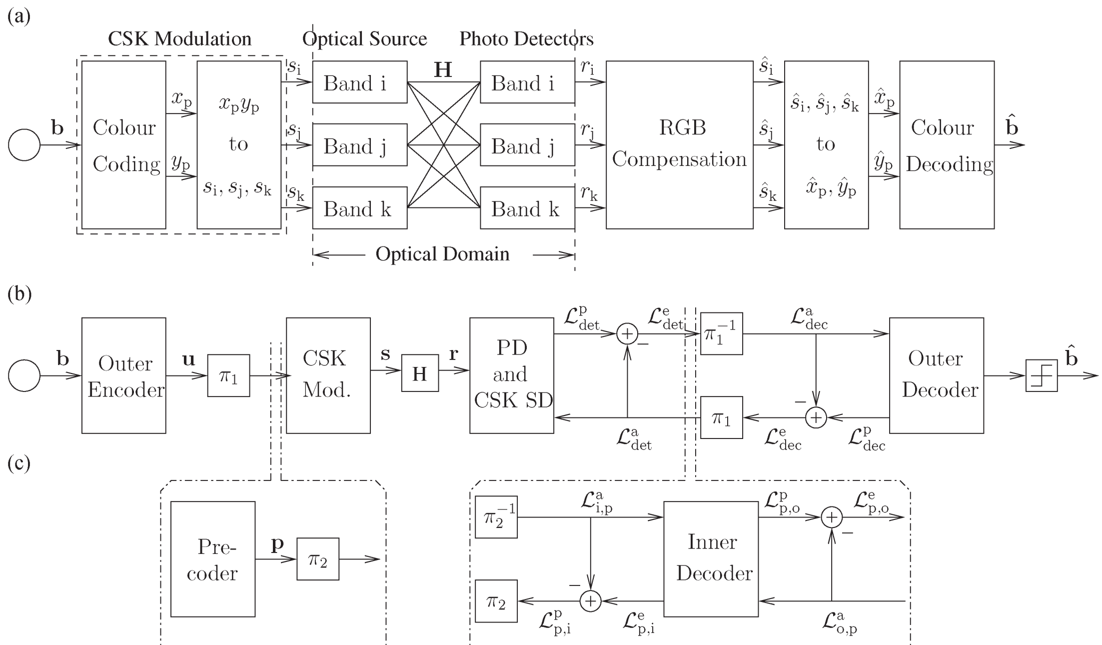

Fig. 1. Transceiver of M-CSK using the joint ML-based HD in (a), the two-stage iterative joint MAP-based SD in (b), and the three-stage iterative joint MAP-based SD with URC predecoder in (c).

on EXIT chart-based constellation labeling. We then design sophisticated channel coding schemes for achieving a near-capacity performance. Our performance versus coding complexity results and the practically achievable physical transmission distance are also discussed. Finally, we conclude in Section IV.

Notations: In this paper, we use lowercase bold fonts to represent a vector, and uppercase bold fonts to denote a matrix, where we let the superscript in bracket $()^{(n)}$ denote the nth candidate in all possible legitimate intensity vectors. Additionally, the operator $\mathbb{E}$ stands for expectation and $\mathbb{T}$ for the SD transfer function; $\mathcal{Q}$ is the Q-function, which is used for error probability calculation; $()^T$ represents the matrix transpose; and $\|\|$ denotes the Euclidean norm. Finally, we employ $\mapsto$ to represent the misinterpretation of a received symbol as another one in our pairwise error probability (PEP) calculation.

II. Color Shift Keying System

Fig. 1 shows the transceiver architecture of M-ary CSK. Explicitly, in Fig. 1(a), the joint ML-based HD-aided system is presented, whereas our two-stage joint MAP-based SD-aided system is shown in Fig. 1(b). As proposed in the IEEE 802.15.7 standard [16], the M-ary color coding scheme groups the consecutive $N_b = \log_2 M$ incoming bits $\mathbf{b}$ into M-ary CSK symbols mapped onto a 2-D color constellation point in the form of the xy color coordinate set $(x_p, y_p) \in \chi$, where χ contains all the xy color coordinate set. The color coordinates $\mathbf{x} = (x_p, y_p)$ are generated by the intensity of the three light sources; hence, these xy color coordinates are converted to the three-element optical intensity vectors $\mathbf{s}_n = [s_i, s_j, s_k]^T$ before transmission, which represent the power of the light sources.

A. CSK Modulation

1) Color Coding: The color constellations[1] of 8-CSK and 16-CSK are displayed in Fig. 2, where the aforementioned xy color coordinates represent the specific locations of the CSK symbols (marked by $c_\xi,\ \xi = 1, \ldots, M$). The operating light intensity I is normalized to unity. Since CSK operates at a fixed intensity, a constraint is imposed on the maximum output light intensity I [19]. Furthermore, for the sake of fixing the perceived color, we impose an average color constraint on the CSK symbols for the color as follows [21]:

$$\sum_n \omega_n \mathbf{s}_n = \mathcal{C}_{\text{avg}} \tag{1}$$

where ω_n is the probability of $\mathbf{s}_n$, and $\mathcal{C}_{\text{avg}}$ is a vector representing the average perceived color of the transmitted light, which is known as *color balance*. To elaborate a little further, there is a pair of 2-D color constellations discussed in this paper. Specifically, in *Type I*, the color constellation obeys the IEEE standard of [16], whereas in *Type II*, we rely on a color-balanced constellation, where $\mathcal{C}_{\text{avg}}$ represents a specific perceived color. Specifically, in this paper, we employed a *white-balanced* (WB) color constellation.

The 8-CSK and 16-CSK *Type I* color constellations are portrayed in Fig. 2(a) and (b). By contrast, in Fig. 2(c) and (d), the 8-CSK and 16-CSK *Type II* color constellations maintaining WB [19], [21] are presented. Owing to the constellation

[1]The constellation is a collection of xy coordinates, which is defined by the international commission on illumination in CIE 1931 color space of [29], where each location corresponds to a color with a specific wavelength, as perceived by the human eye. The location of constellation points may be on the edge, on the vertices, or within a triangle where the vertices represent the optical light sources, as detailed in [17].

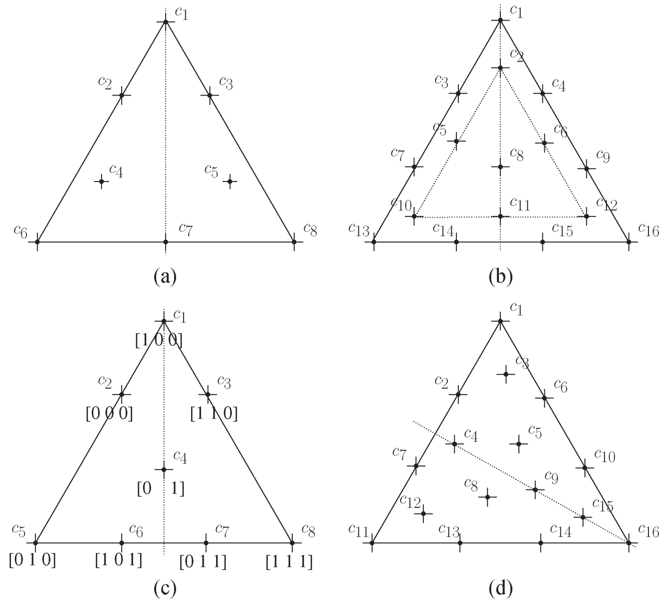

Fig. 2. Color constellation of 8-CSK and 16-CSK, where the operating intensity is normalized to 1. The CSK color constellations specified by the IEEE standard [16] *Type I* are detailed in (a) and (b), whereas those of (c) and (d) are the WB constellations *Type II* proposed in [21]. The details of (c) will be further explained in Table I as an example.

simplicity of 4-CSK, the standard color constellation automatically retains the WB property. Having considered these two types of constellations, the bits $\mathbf{b}$ are mapped to the corresponding xy color coordinates according to the signal labeling strategy of $\mu^l(\mathbf{b}) \rightarrow (x_p, y_p)$, where l denotes the lth possible signal labeling strategy of all possible candidates, and our specific signal labeling design will be detailed in Section III-A.

2) Light Intensity Conversion: The 2-D xy color coordinates of the symbols are now converted to the 3-D optical signal intensities of light bands. We let $\mathcal{S}$ denote the alphabet of the transmitted intensity vector $\mathbf{s}_n$. The subsequent conversion to the optical signal intensities of the source light is achieved by simultaneously solving a simple system of three equations, i.e., $\{\mathbf{x}_p = \mathbf{x}_c^T\mathbf{s}; y_p = \mathbf{y}_c^T\mathbf{s}; \sum \mathbf{s} = I\}$, where we define the coordinate vector of the three light sources as $\mathbf{x}_c = [x_i, x_j, x_k]^T$ and $\mathbf{y}_c = [x_i, x_j, x_k]^T$ [16]. Thus, the entire CSK modulation process may be interpreted as a one-to-one mapping function.

Example: For the 8-CSK *Type II* color constellation of Fig. 2(c), given the color band combinations of $[110, 010, 000]$,[2] the basic coordinates are $\mathbf{x}_c = [0.734, 0.402, 0.169]$ and $\mathbf{y}_c = [0.265, 0.597, 0.007]$, whereas the corresponding color constellations χ in the dimensions $\mathbf{x} = (x_p, y_p)$ are shown in Table I.

Then, upon solving the given system of equations, we arrive at the alphabet of intensity vectors $\mathbf{s}$, where an example of the 8-CSK's intensity vector alphabet $\mathcal{S}$ (columns of s_i, s_j, and s_k) is included in Table I. Furthermore, the notations $\mathcal{S}_{u1}^0$ and $\mathcal{S}_{u1}^1$ are only relevant for SD-aided CSK, which will be detailed in

[2]The IEEE standard [16] proposed nine valid sets of color band combinations, where each combination represents a set of three potential color schemes to be used in the CSK system. For example, the color band [110, 010, 000] corresponds to the specific color source, which has the center wavelength of 753, 564, and 429 nm [17].

TABLE I
ALPHABET OF 8-CSK *Type II* INTENSITY VECTORS $\mathcal{S}$, USING THE COLOR BAND COMBINATION OF [110, 010, 000]

	$\mathbf{b}$	label	$\mathbf{x} = (x_\text{p}, y_\text{p})$	s_i	s_j	s_k
$\mathcal{S}_{u_1}^0$	000	c_2	$(0.435, 0.299)$	0	0.666	0.334
	001	c_4	$(0.513, 0.486)$	0.112	0.278	0.610
	010	c_5	$(0.324, 0.400)$	0.610	0.279	0.111
	011	c_7	$(0.402, 0.597)$	0.501	0	0.499
$\mathcal{S}_{u_1}^1$	100	c_1	$(0.357, 0.093)$	0	1	0
	101	c_6	$(0.546, 0.179)$	0	0	1
	110	c_3	$(0.169, 0.007)$	0.334	0.666	0
	111	c_8	$(0.734, 0.265)$	1	0	0

Section II-D. As for other CSK modulation schemes, a similar procedure will be implemented.

B. Optical Domain Propagation

In this paper, we consider a point-to-point transmission system, where the optical signal intensities $\{s_i, s_j, s_k\}$ of the three light bands $\{i, j, k\}$ emitted from the M-CSK modulator block of Fig. 1(a) propagate through an optical channel. At the receiver, a dedicated photodetector (PD) corresponding to each of the three light bands is used for converting the received color component into their electronic representations. Explicitly, the output $\mathbf{r}$ is a distorted and noise-contaminated intensity vector of the color light bands formulated as

$$\mathbf{r} = \mathbf{H}\mathbf{s} + \mathbf{v}. \qquad (2)$$

The optical channel is subjected to potential color-band interference; hence, $\mathbf{H}$ is a (3×3)-element matrix, where the diagonal entries of $\mathbf{H}$ represent the channel gain of the corresponding band, whereas the other entries host the interference imposed by the other bands. As pointed out in [24], other propagation factors, such as diffuse multipath, dispersion, and the non-LOS components, should also be considered in the future, but again, 90% of the received power is concentrated in the LOS component, whereas the contribution of the power received from reflections is small enough to be neglected. Therefore, the channel matrix may be assumed an idealized identity matrix. Based on these discussions, in this paper, we assume that the system experiences an ideal AWGN channel.

Furthermore, $\mathbf{v}$ represents the noise imposed in the electronic domain at the receiver, with each entry having a zero mean and a variance of $\sigma_0^2 = \sigma^2/3$, where we define the electronic SNR as $1/\sigma^2$ and σ^2 is the total electronic domain noise power at the receiver. Thus, we have $E_{b_\text{elec.}}/N_0 = 1/(N_b\sigma_0^2)$. Furthermore, we may also conveniently define the optical SNR as $\gamma_o = \kappa\gamma_e$, where $\kappa = \sigma\mathbb{E}\{\|\mathbf{s}\|\}/\mathbb{E}\{\|\mathbf{s}\|^2\}$.

C. Joint ML-Based CSK HD of the Three Colors

In practice, all the aforementioned detrimental channel effects can be mitigated by the RGB compensation block of Fig. 1(a) for retrieving the transmitted optical intensities.[3]

[3]Note that we implicitly assumed here lossless conversion from the electronic domain to the optical domain at the transmitter and from the optical domain to the electronic domain at the receiver. Hence, we may use the optical signal intensity and electronic signal amplitude interchangeable.

When we assume perfect channel state information (CSI) at the receiver, the estimated intensity vector $\tilde{\mathbf{s}}$ is obtained by the joint ML-based HD of the three colors. When an order value of $M = 4, 8, 16$ is considered, the full-search-based joint ML detection complexity remains moderate, and the estimated intensity vector may then be expressed as

$$\hat{\mathbf{s}} = \arg\min_{\tilde{\mathbf{s}}\in\mathcal{S}} \|\mathbf{r} - \mathbf{H}\tilde{\mathbf{s}}\|^2 \tag{3}$$

which implies that the estimated intensity vector $\hat{\mathbf{s}}$ is given by that specific legitimate intensity vector $\tilde{\mathbf{s}} \in \mathcal{S}$, which exhibits the lowest distance between $\mathbf{r}$ and $\mathbf{H}\tilde{\mathbf{s}}$. The estimated intensity vector $\hat{\mathbf{s}}$ is then finally converted back to the resultant bits.

Let us now characterize the analytical performance of our joint ML-based HD by the union-bound-based approach for deriving an upper bound, which may be deemed tight at high SNRs, where the average bit error probability may be written as [30]

$$P_{e,\text{union}} \le \frac{1}{MN_b}\sum_{\xi=1}^{M}\sum_{\zeta=1,\zeta\neq\xi}^{M} d\left(\tilde{\mathbf{s}}^{(\xi)}, \tilde{\mathbf{s}}^{(\zeta)}\right) P\left(\tilde{\mathbf{s}}^{(\xi)} \mapsto \tilde{\mathbf{s}}^{(\zeta)}\right) \tag{4}$$

with $d(\tilde{\mathbf{s}}^{(\xi)}, \tilde{\mathbf{s}}^{(\zeta)})$ representing the Hamming distance of the legitimate intensity vectors $\tilde{\mathbf{s}}^{(\zeta)}$ and $\tilde{\mathbf{s}}^{(\zeta)}$. Furthermore, $P(\tilde{\mathbf{s}}^{(\xi)} \mapsto \tilde{\mathbf{s}}^{(\zeta)})$ denotes the PEP of these legitimate intensity vectors, which is given by [30]

$$\begin{aligned} P&\left(\tilde{\mathbf{s}}^{(\xi)} \mapsto \tilde{\mathbf{s}}^{(\zeta)}\right)\\ &= P\left[\left\|\mathbf{r}-\mathbf{H}\tilde{\mathbf{s}}^{(\xi)}\right\|^2 > \left\|\mathbf{r}-\mathbf{H}\tilde{\mathbf{s}}^{(\zeta)}\right\|^2\right]\\ &= P\left[\left\|\mathbf{H}\tilde{\mathbf{s}}^{(\xi)}\right\|^2\Big/2-\mathbf{r}^T\mathbf{H}\tilde{\mathbf{s}}^{(\xi)} > \left\|\mathbf{H}\tilde{\mathbf{s}}^{(\zeta)}\right\|^2\Big/2-\mathbf{r}^T\mathbf{H}\tilde{\mathbf{s}}^{(\zeta)}\right]\\ &= P\left[\left(\mathbf{H}\tilde{\mathbf{s}}^{(\xi)}+\mathbf{v}\right)^T \mathbf{H}\left(\tilde{\mathbf{s}}^{(\zeta)}-\tilde{\mathbf{s}}^{(\xi)}\right)\right.\\ &\qquad\left. > \frac{\left\|\mathbf{H}\tilde{\mathbf{s}}^{(\zeta)}\right\|^2-\left\|\mathbf{H}\tilde{\mathbf{s}}^{(\xi)}\right\|^2}{2}\right]\\ &= P\left[\mathbf{v}^T\mathbf{H}\left(\tilde{\mathbf{s}}^{(\zeta)}-\tilde{\mathbf{s}}^{(\xi)}\right) > \Psi\right] \end{aligned} \tag{5}$$

where we have

$$\Psi = \left(\left\|\mathbf{H}\tilde{\mathbf{s}}^{(\zeta)}\right\|^2 - \left\|\mathbf{H}\tilde{\mathbf{s}}^{(\xi)}\right\|^2\right)\Big/2 - \left(\mathbf{H}\tilde{\mathbf{s}}^{(\xi)}\right)^T\mathbf{H}\left(\tilde{\mathbf{s}}^{(\zeta)}-\tilde{\mathbf{s}}^{(\xi)}\right). \tag{6}$$

Since $\mathbf{H}(\tilde{\mathbf{s}}^{(\zeta)} - \tilde{\mathbf{s}}^{(\xi)})$ is a matrix that contains constant numbers, the term $\mathbf{v}^T\mathbf{H}(\tilde{\mathbf{s}}^{(\zeta)} - \tilde{\mathbf{s}}^{(\xi)})$ obeys the Gaussian distribution with $\mathcal{N}(0, \|\mathbf{H}\tilde{\mathbf{s}}^{(\zeta)} - \mathbf{H}\tilde{\mathbf{s}}^{(\xi)}\|^2\sigma_0^2)$. As a result, the PEP between $\tilde{\mathbf{s}}^{(\xi)}$ and $\tilde{\mathbf{s}}^{(\zeta)}$ can be written as

$$P\left(\tilde{\mathbf{s}}^{(\xi)} \mapsto \tilde{\mathbf{s}}^{(\zeta)}\right) = \mathcal{Q}\left(\Psi\Big/\left\|\mathbf{H}\tilde{\mathbf{s}}^{(\zeta)} - \mathbf{H}\tilde{\mathbf{s}}^{(\xi)}\right\|\sigma_0\right). \tag{7}$$

D. Joint MAP-Based CSK SD of the Three Colors

Let us now discuss the more powerful joint MAP-based SD of M-CSK and its iterative receiver shown in Fig. 1(b). When a sophisticated channel-coded system is considered, the information bit sequence $\mathbf{b}$ is first channel encoded, yielding the coded bit sequence $\mathbf{u}$ and then bit-interleaved by π_1, before entering into the M-CSK block. The subsequent one-to-one mapping of Fig. 1(b) from the incoming bits to the resultant optical light intensities follows the procedure detailed in Section II-A. Following the PDs employed at the receiver's front end in Fig. 1(b), a joint MAP-based SD block is used for directly converting the received optical signal intensities back to channel-coded soft values, rather than going through the consecutive stages of RGB compensation, demapping, and color decoding, which was required when joint ML-based HD was employed.

The joint MAP-based SD block of Fig. 1(b) exchanges *extrinsic* information with the channel decoder, and the final HD is carried out by the channel decoder once a predefined stopping criterion, such as the maximum affordable number of iterations, has been met. For ease of explanation, the following terms are defined:

- $\mathcal{L}_{\text{det}}^{p}$, $\mathcal{L}_{\text{det}}^{a}$, and $\mathcal{L}_{\text{det}}^{e}$: the *a posteriori*, *a priori*, and *extrinsic* log-likelihood ratio (LLR) of the detection block, which are detailed in [25] and [27].
- $\mathcal{L}_{\text{dec}}^{p}$, $\mathcal{L}_{\text{dec}}^{a}$, and $\mathcal{L}_{\text{dec}}^{e}$: the *a posteriori*, *a priori*, and *extrinsic* LLR of the channel decoder block.

Recall that the M-CSK scheme groups a set of $N_b = \log_2 M$ consecutive incoming bits, when we consider $\mathbf{u}_{(1:N_b)}$ to be a binary sequence constituted by N_b consecutive bits. Then, for the vth bit of $\mathbf{u}_{(1:N_b)}$, its bit-wise *a posteriori* information $\mathcal{L}_{\text{det}}^{p}(u_v)$ can be derived by the max-log approximation, i.e., [31]

$$\begin{aligned} \mathcal{L}_{\text{det}}^{p}(u_v) = \mathcal{L}_{\text{det}}^{a}(u_v) &+ \max_{\tilde{\mathbf{s}}\in\mathcal{S}_{u_v}^{1}}\left[-\|\mathbf{r}-\mathbf{H}\tilde{\mathbf{s}}\|^2/2\sigma^2 + A\right]\\ &- \max_{\tilde{\mathbf{s}}\in\mathcal{S}_{u_v}^{0}}\left[-\|\mathbf{r}-\mathbf{H}\tilde{\mathbf{s}}\|^2/2\sigma^2 + A\right] \end{aligned} \tag{8}$$

where we introduce the shorthand of $A = \sum_{\tau=1,\tau\neq v}^{N_b} u_v\mathcal{L}_{\text{det}}^{a}(u_\tau)$ for compactness. Additionally, we define $\mathcal{S}_{u_v}^{0}$ and $\mathcal{S}_{u_v}^{1}$ as two subsets of $\mathcal{S}$, namely as $\mathcal{S}_{u_v}^{0} = \{\tilde{\mathbf{s}} \in \mathcal{S} | u_v = 0\}$ and $\mathcal{S}_{u_v}^{1} = \{\tilde{\mathbf{s}} \in \mathcal{S} | u_v = 1\}$, where a simple subset example is given in Table I.

As a result, the *extrinsic* LLRs $\mathcal{L}_{\text{det}}^{e}$ gleaned from the detection block of Fig. 1(b) are deinterleaved, and then they are fed as the *a priori* LLRs $\mathcal{L}_{\text{dec}}^{a}$ into the outer decoder of Fig. 1(b). Similarly, as shown in Fig. 1(b), the updated *extrinsic* LLRs $\mathcal{L}_{\text{dec}}^{e}$ are fed back and reinterleaved, before being processed as the *a priori* LLRs $\mathcal{L}_{\text{det}}^{a}$ by the detection block [32].

III. Extrinsic Information Transfer-Chart-Aided Analysis

Having obtained the soft LLRs of the joint MAP-based SD, let us now invoke EXIT charts [25] for conveniently analyzing the convergence behavior of our iterative-detection-aided coded

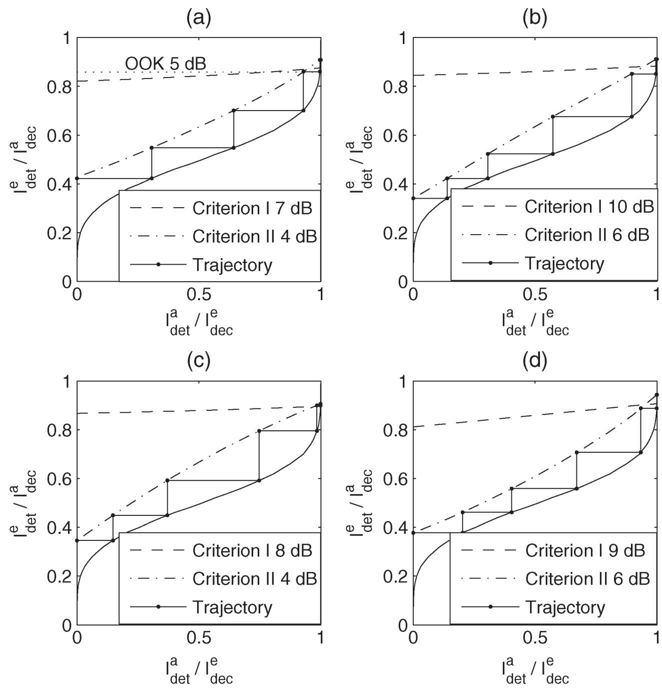

Fig. 3. EXIT characteristics of CSK joint MAP-based SD using different color constellations in an AWGN channel and a half-rate RSC outer decoder (solid line). In all figures, the dashed line and the dash-dotted line represent the approximately required minimum electronic $E_{b_{\text{elec.}}}/N_0$ (detailed in legend) to provide an open tunnel for Criteria I and II, and ON–OFF keying (OOK) is added as benchmarker. (a) 8-CSK *Type I*. (b) 16-CSK *Type I*. (c) 8-CSK *Type II*. (d) 16-CSK *Type II*.

M-CSK system by examining the exchange of the input/output mutual information I^a_{det} and I^e_{det} between the inner and outer decoders [25]. To be more explicit, by investigating the EXIT characteristics and the area of open EXIT of the tunnel between the EXIT curves of the inner and outer decoders, we were able to find the most beneficial signal labeling for diverse design objectives. In the remainder of this paper, we assume familiarity with EXIT charts; see [27].

A. Design Criterion I

Fig. 3 portrays the EXIT characteristics of 8-CSK and 16-CSK employing both types of color constellations of Fig. 2 for transmission over a LOS AWGN channel, where the S-shaped solid lines represent the EXIT characteristics of a half-rate recursive systematic convolutional (RSC) outer decoder, whereas the dashed or dash-dotted lines represent the specific SNR values, where an open EXIT chart tunnel emerges.

For the time being, let us focus our attention on the dashed lines in Fig. 3. The most important observation related to M-CSK is that its EXIT characteristic exhibits a modest but perceivable slope, which implies that the employment of an iterative receiver is capable of providing some iteration gain in M-CSK. By contrast, as shown in Fig. 3(a), OOK does not exhibit any iteration gain. This is because the OOK bits of the three emitters are independent of each other; hence, they provide no extrinsic information for each other. On the other hand, the bits of the CSK symbols are not independent of each other; hence, a modest iteration gain is achieved. However, the gradient of the joint MAP-based SD's curve is low. This is because the signal labeling design of [16] minimizes the sum of Hamming distances between the pair of the closest adjacent color constellation points of 8-CSK and 16-CSK. To elaborate a little further, the bit-to-symbol mapping rule, which is also referred to as the constellation labeling μ of the 8-CSK and 16-CSK schemes obeying Criterion I, is formulated as

TABLE II
LABELING MAPS PRESENTED FOR DIFFERENT CONSTELLATION AND DETECTION SCHEMES

name	labels ($c_1 \cdots c_{N_b}$) in Fig. 2
8-CSK *Type I*, **Crit. I**	(4,0,6,1,2,5,3,7)
8-CSK *Type I*, **Crit. II**	(2,5,1,0,4,3,7,6)
8-CSK *Type II*, **Crit. I**	(3,2,1,0,6,4,5,7)
8-CSK *Type II*, **Crit. II**	(2,1,7,4,5,6,3,0)
16-CSK *Type I*, **Crit. I**	(0,1,3,5,2,7,10,6,4,11,14,13,9,15,12,8)
16-CSK *Type I*, **Crit. II**	(7,1,5,8,9,15,0,3,14,11,10,4,12,2,6,13)
16-CSK *Type II*, **Crit. I**	(1,0,3,5,4,2,7,13,12,6,15,9,10,14,11,8)
16-CSK *Type II*, **Crit. II**	(8,14,13,4,1,3,10,7,11,6,9,12,0,15,5,2)

$$\textbf{Criterion I: } \tilde{\mu}^l_{\text{I}} = \arg\min_{\mu^l \in \mathbb{M}} \sum_{1}^{M} d_{\text{adj}}(\mu^l) \tag{9}$$

where $\mathbb{M}$ denotes an $(M! \times M)$-element matrix, each row of the matrix contains a set of legitimate signal labelings (signal labeling examples can be found in Table II), d_{adj} represents the Hamming distance between the adjacent color constellation points, and μ^l is the specific signal labeling. We launch a full search within the set $\mathbb{M}$ and choose the specific signal labeling that meets the requirement of (9). We invoke this criterion for designing a Gray-coded bit-to-symbol mapping for *Type II* color constellations, noting that, due to the specific arrangement of the color constellation points shown in Fig. 2, it is impossible to realize a perfect and consistent Gray bit-to-symbol mapping. Explicitly, our proposed signal labeling designed for the *Type II* color constellation using Criterion I is listed in Table II, where the decimal numbers represent the corresponding bit combinations, which are assigned to their corresponding locations $(c_1, c_2, \ldots, c_8)$ in Fig. 2. Additionally, when using this criterion, we obtained the same signal labeling scheme as the IEEE standard constellation labeling of [16].

Fig. 4 portrays the BER performance of the joint ML-based HD-aided CSK system of Fig. 1(a) using different color constellations and signal labeling strategies in an AWGN channel. Observe in Fig. 4 that all our simulation results recorded for the *Type I* color constellation of $M = 4, 8$, and 16-CSK using Criterion I are well matched to their analytical union bound represented in dashed line.

B. Design Criterion II

1) Design Criterion: When we design the signal labeling for our iterative joint MAP-based SD-aided receiver, the bit-to-symbol mapping is different from the Gray-like mapping of Criterion I. In general, when an iterative receiver is invoked, the free squared Euclidean distance condition (FEDC) on having ideal feedback usually dominates the performance of iterative detection system [33], [34]; hence, a signal labeling having a large FEDC performs well.

Additionally, in [33], an alternative objective function (OF) is proposed for the constellation labeling search procedure relying

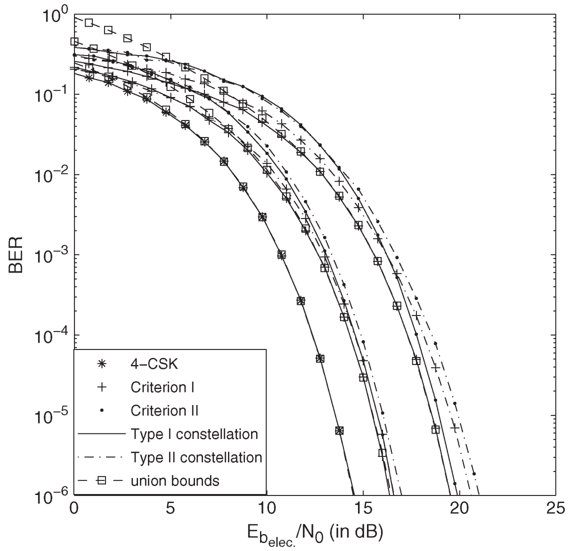

Fig. 4. Analytical and empirical BER performance of the joint ML-based HD CSK schemes using both types of color constellations and different signal labeling strategies in an AWGN channel. The corresponding three- and four-bits/symbol constellation layouts are described in Fig. 2, and the various signal labeling schemes are detailed in Table II. The analytical union bounds are represented by the dashed lines and squares.

on the *harmonic mean* of the minimum squared Euclidean distance after the feedback, which is formulated as [34]

$$d_h^2(\mu) = \left(\frac{1}{N_b 2^{N_b}} \sum_{n=1}^{N_b} \sum_{b=0}^{1} \sum_{\mathbf{x} \in \chi_b^n} \frac{1}{\|\mathbf{x} - \mathbf{z}\|^2} \right)^{-1} \tag{10}$$

where χ_b^n is the specific subset of χ, whose label has the binary value b at the nth bit position, whereas $\mathbf{z}$ is the same as $\mathbf{x}$, except that its nth bit is inverted. As pointed out in [33] and [34], a specific signal labeling associated with a large d_h^2 usually also has a large FEDC; hence, we rely on the d_h^2 OF value for characterizing a signal labeling, rather than on the computationally more complex evaluation of the FEDC.

However, purely relying on evaluating the FEDC value alone is insufficient because it does not guarantee finding near-capacity signal labelings, as also pointed out in [35]. Namely, our goal is to find that specific signal labeling, which leads to the smallest open tunnel area in the EXIT chart [34], [35]. Hence, in this paper, we first evaluate all legitimate the signal labeling schemes based on (10) and then verify the result with the aid of EXIT chart analysis.

Example: Given the 8-CSK *Type II* color constellation of Fig. 2(c), based on studying the Hamming distance between the closest-neighbor adjacent constellation points, we carried out a full search in the space of all possible $M!$ signal labeling possibilities and used the one associated with the largest d_h^2 OF value, while relying on the design criterion of

$$\textbf{Criterion II: } \widetilde{\mu}_{\text{II}}^l = \arg\max_{\mu^l \in \mathbb{M}} d_h^2(\mu^l). \tag{11}$$

The resultant signal labeling designed for the for 8-CSK *Type II* color constellation relying on our iterative joint MAP-based SD-aided receiver is also shown in Table II. For other

TABLE III
EXAMPLE OF OPTIMIZING SIGNAL LABELING CANDIDATES FOLLOW CRITERION II FOR 8-CSK TYPE II COLOR CONSTELLATION

name	labels ($c_1 \cdots c_{N_\text{b}}$)	d_h^2	open tunnel	$\mathcal{A}_\text{diff}$
Label 1	(7,3,6,0,2,1,5,4)	0.0653	6.5 dB	0.3166
Label 2	(4,1,2,6,7,0,3,5)	0.1217	4.0 dB	0.1625
Label 3	(4,1,5,0,3,2,6,7)	0.0519	7.5 dB	0.3694
Label 4	(7,4,2,0,3,5,6,1)	0.0934	4.5 dB	0.1951
Label 5	(4,5,7,0,3,6,2,1)	0.0763	5.5 dB	0.2582
proposed	(2,1,7,4,5,6,3,0)	0.1280	3.5 dB	0.1333

CSK color constellations using joint MAP-based SD, the signal labeling design follows the same procedure, which has also been detailed in Table II. Inspired by the method of [28], we use EXIT charts for comparing the performance of the signal labeling schemes employed.

2) EXIT-Chart-Based Verification of the d_h^2-Aided Labeling Optimization: It was shown in [28] that the area under the EXIT curve of a joint MAP-based SD's EXIT chart approximately equals to the system's achievable throughput, which is directly related to its electronic SNR, but remains unaffected by its signal labeling, i.e., [25]

$$\mathcal{A}(\gamma_e) = \int_0^1 I_{\text{det}}^e \, dI_{\text{det}}^a \tag{12}$$

$$= \int_0^1 \mathbb{T}_{\text{det}} \left(I_{\text{det}}^a, \mu^l, \gamma_e \right) dI_{\text{det}}^a. \tag{13}$$

Furthermore, the area under the outer decoder's EXIT curve equals to its coding rate R. Again, if we expect the system to achieve a vanishingly low BER, it has to exhibit an open tunnel all the way, leading to the (1.0, 1.0) point. Then, the open tunnel area $\mathcal{A}_\text{diff}$ between these two curves characterizes the system's binary data-rate loss in comparison to its true capacity, and the size of this area depends on the specific the signal labeling [28]

$$\mathcal{A}_\text{diff}(\mu^l, \gamma_e) = \mathcal{A}(\gamma_e) - R. \tag{14}$$

If we aim to attain a near-capacity performance, the area $\mathcal{A}_\text{diff}$ should be small. Based on (14), we proceed by finding the specific signal labeling strategy that results in having an open EXIT tunnel at the lowest possible electronic SNR, which leads to a vanishingly low BER at the lowest SNR, provided that the interleaver is sufficiently long to ensure that the soft information is near Gaussian. For practical finite-length interleavers, this is not the case; hence, usually, a slightly higher SNR is required for the stair-case-shaped decoding trajectory to pass through the EXIT chart's constriction. To demonstrate the associated $\mathcal{A}_\text{diff}$ differences, we consider the 8-CSK *Type II* color constellation as an example and randomly opt for the signal labeling schemes of Table III. When we invoke a half-rate RSC code, the corresponding results are shown in Fig. 5, whereas some specific numerical results are listed in Table III. Observe in Fig. 5 that the EXIT characteristics of the randomly selected Labels 1–5 exhibit different gradients and that our proposed signal labeling has the smallest open tunnel, as well

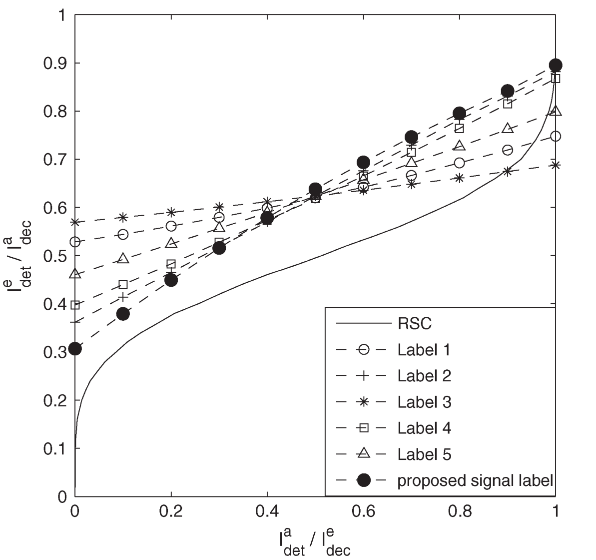

Fig. 5. EXIT characteristics of our proposed signal labeling candidates for 8-CSK *Type II* at $E_{b_{\text{elec.}}}/N_0 = 3.5$ dB (dashed lines) for joint MAP-based SD for our iterative receiver of Fig. 1(b) in an AWGN channel, where the solid S-shaped line represents the half-rate RSC decoder, whereas the index of the different signal labeling strategies has been detailed in Table III.

as a crossover point closest to the (1.0, 1.0) point, which implies having the lowest residual BER, as detailed in [25]–[27]. The tunnel opens at $E_{b_{\text{elec.}}}/N_0 = 3.5$ dB, whereas for the other signal labeling schemes, the EXIT characteristics intersect with that of the outer decoder. This suggests that our proposed signal labeling is capable of achieving a significant iteration gain. Following this approach, our other proposed signal labeling schemes are listed in Table II.

3) Performance Comparison of Criteria I and II: Let us now return to Fig. 3 and observe the dash-dotted lines in each subfigure, which represent the EXIT characteristics of the labeling schemes obeying Criterion II. For all color constellations, the dash-dotted style curves are associated with a steeper gradient and a lower open-tunnel area than for Criterion I. This implies that the reliability of the *extrinsic* LLRs improves more substantially upon iterating since more reliable *a priori* LLRs are gleaned from the outer decoder. Furthermore, the dash-dotted lines cross the S-shaped RSC decoder curves closer to the (1.0, 1.0) point; hence, a lower residual BER floor is expected. Having said this, we also note that these benefits are achieved at the cost of an increased number of iterations, i.e., at higher complexity.

Furthermore, as for the performance of Criterion II using HD shown in Fig. 4, we can observe that, although the differences between the designs relying on Criteria I and II are relatively small, the performance of the signal labeling obeying Criterion I is consistently better than that of Criterion II. This is because having the lowest Hamming distance between the points of closest-neighbor adjacent constellation points ensures having the least number of bit errors between the adjacent constellation points, when decision errors occur in an AWGN channel. Moreover, regardless of the specific signal labeling criterion used, the *Type II* color constellation is outperformed by the color constellation *Type I*. Hence, in line with [21] and [22], the color constellation *Type I* is confirmed to be a better solution for an uncoded CSK system.

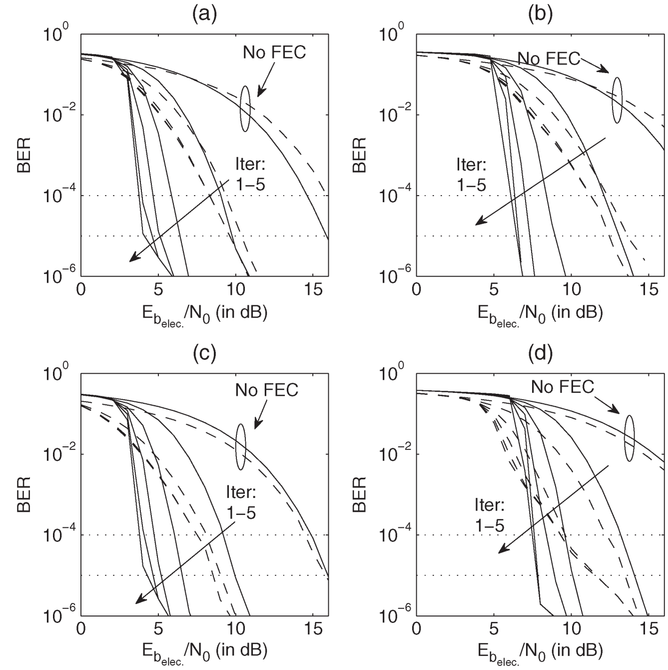

Fig. 6. BER performance of the two-stage half-rate RSC coded CSK system of Fig. 3 using our joint MAP-based SD-aided iterative receiver, where different color constellations are considered. Criterion I is represented by the dashed line and Criterion II by the solid line. From right to left, the multiple solid and dashed lines represent the BER curves associated with an increasing number of iterations from 1 to 5 (link to Fig. 3). (a) 8-CSK *Type I*. (b) 16-CSK *Type I*. (c) 8-CSK *Type II*. (d) 16-CSK *Type II*

Additionally, the corresponding BER characteristics of Fig. 3 are shown in Fig. 6,[4] where both the *Types I* and *II* color constellations of Fig. 2 are characterized in an AWGN channel, and both Criteria I and II are considered. Similarly to our EXIT-chart-based predictions shown in Fig. 3, the different M-CSK schemes exhibit rather different iteration gains in Fig. 6. The maximum attainable iteration gain of the systems relying on Criterion I is essentially achieved during the first two rounds, which is due to the limited slope of the related EXIT curves shown by the dashed lines in Fig. 3. By contrast, the systems relying on Criterion II benefit from a more substantial iteration gain. Consequently, the shape of the BER curves exhibits a "turbo-cliff" effect. After five iterations, the electronic SNR difference between the two different signal labeling schemes is around 5–7 dB in all subfigures.

Another important observation in Fig. 6 is that there is a gradient change in the BER curves around 10^{-5}, as mentioned in Section III-C. This point is associated with the intercept point observed in the EXIT chart of Fig. 3. Hence, the EXIT characteristic of the joint MAP-based SD scheme fails to reach the (1.0, 1.0) point. We will demonstrate in Section III-C that this performance limitation is almost completely eliminated by our three-stage system.

[4]Although introducing a redundant forward error correction (FEC) code reduce the effective data rate of the system, it results in considerable performance gains. Furthermore, in [16], half-rate or even lower rate Reed–Solomon codes were considered, which is outperformed by the FEC scheme employed in this paper.

C. Three-Stage Concatenated Error Correction Coding

Again, despite the aforementioned benefits, all the EXIT characteristics of the iterative joint MAP-based SD schemes fail to reach the (1.0, 1.0) point at the top-right corner of the EXIT chart, which implies the potential emergence of an error floor in the low BER range. Suffice it to say here that it was demonstrated in [25]–[27] that an open EXIT tunnel leading to the (1.0, 1.0) point of the EXIT chart is a sufficient condition for achieving iterative decoding convergence to a vanishingly low BER. Invoking an additional unity-rate code (URC) is capable of eliminating this problem, as detailed in [25]–[27], because it has an infinite impulse response and, hence, efficiently spreads the *extrinsic* information without increasing the system's interleaver delay. Due to its unity rate and simple two-stage trellis, this is achieved without reducing the throughput while only modestly increasing the complexity.

Hence, this becomes a three-stage concatenated system, where a URC encoder and decoder along with their interleaver and deinterleaver are inserted at the transmitter and receiver, respectively, as shown in Fig. 1(c). At receiver end, we first perform a sufficiently high number of iterations between the joint MAP-based SD and the URC decoder, which we refer to as inner iterations. The output $\mathcal{L}_{p,o}^{p}$ of this combined block is then forwarded to the outer RSC decoder for exchanging the LLRs. The outer decoder then provides *extrinsic* information in form of the *a priori* information $\mathcal{L}_{o,p}^{a}$ fed to the inner decoder. These iterations continue until the maximum affordable number of outer iterations has been reached.

Again, invoking the URC imposes slight extra complexity, but fortunately, the number of inner iterations required remains low. The associated performance of the 8-CSK *Type II* color constellation of Fig. 2(c) is shown in Fig. 7 when we employ two inner iterations between the SD and URC decoder.

In Fig. 7, we use the solid line marked by the square and circle markers for representing the different signal labeling strategies and operating with the aid of the URC precoder. We also portray the corresponding results achieved by our two-stage concatenated system operating without the URC, which is represented by the dashed and dash-dotted lines for comparison. Upon introducing the URC precoder of Fig. 1(c), all the EXIT curves become capable of reaching the (1.0, 1.0) point in Fig. 7, Although, we note that, consequently, we have a starting point in the EXIT curve, which is at a lower value than that of the two-stage system. However, the introduction of this URC does not reduce the overall code rate. Hence, it does not change the area under the EXIT curve of its corresponding three-stage system either. Its ultimate benefit is that it allows the curve to reach the (1.0, 1.0) point. To elaborate a little further, this URC will beneficially affect the shape of the original EXIT curve, making the curve steeper, which may result in a smaller open tunnel area in the EXIT chart, hence requiring a reduced SNR. We note however that it might also increase the risk of intersecting with the outer decoder's curve before it reaches the (1.0, 1.0) point of decoding convergence to an infinitesimally low BER. Hence, it necessitates an increased number of iterations for approaching the (1.0, 1.0) point associated with an infinitesimally low BER. For example, observe furthermore in Fig. 7 that having an open tunnel for Criterion II requires an electronic SNR of 6 dB, whereas Criterion I has an open tunnel at 4 dB for our three-stage system. The same trends are valid for the other three color constellations, which will not be specified here. Correspondingly, the BER performance of Fig. 7 recorded in an AWGN channel is displayed in Fig. 8, where the performance of adopting Criterion I is represented by the dashed line, whereas the solid lines represent Criterion II. The most important result is that the URC precoder eliminates

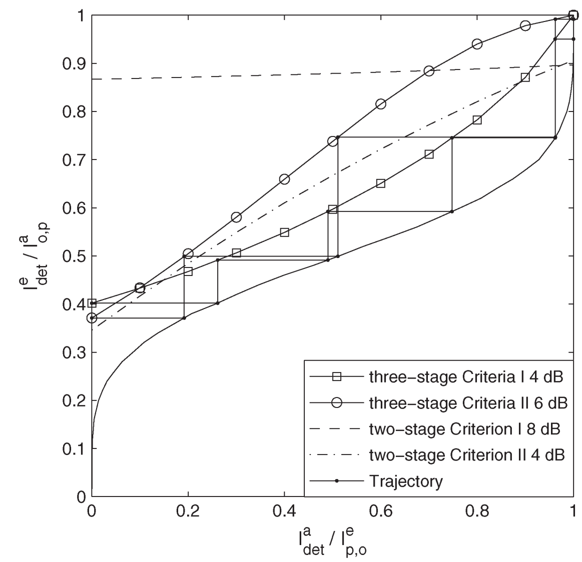

Fig. 7. EXIT characteristics of our joint MAP-based SD assisted 8-CSK *Type II* color constellation with the aid of the URC predecoder after two inner iterations using different color constellations in the AWGN channel and the half-rate RSC outer decoder (solid line), where the solid lines with square and circle markers represent the approximately required minimum electronic $E_{b_{\mathrm{elec.}}}/N_0$ (detailed in legend) to achieve an open tunnel for Criteria I and II, respectively. The dashed and dash-dotted lines denote the EXIT characteristics of the signal labeling adopting Criteria I and II without URC from Fig. 3(c) as our benchmarker.

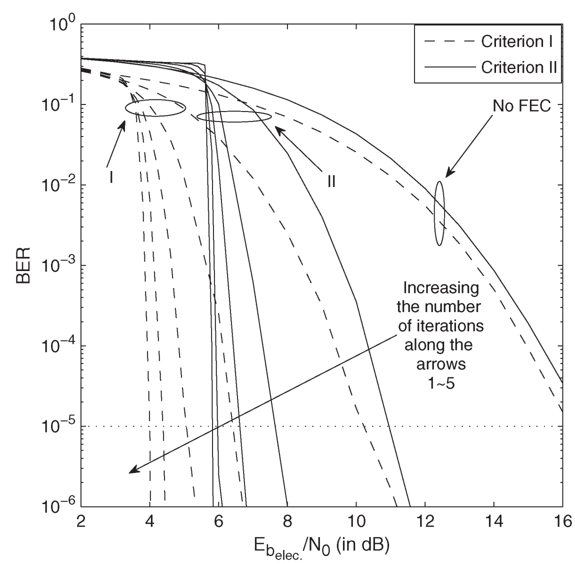

Fig. 8. BER performance of the three-stage half-rate RSC-URC coded CSK system of Fig. 7 using the joint MAP-based SD-aided iterative receiver (two inner iterations), where different color constellations are considered. Criterion I is represented by the dashed line and Criterion II by the solid line. The performance of the system operating without RSC coding is highlighted by an ellipse circle (link to Fig. 7).

TABLE IV
CODING GAIN (dB) OF M-CSK AT BER LEVEL OF 10^{-6}

Constellation labeling	2-stage iterations: 1-5 in [dB]					3-stage iterations: 1-5 in [dB]				
4-CSK	6.4	7.6	7.6	7.6	7.6	5.2	9.6	11.1	11.9	12.2
8-CSK *Type-I* **Criterion I**	6.5	7.2	7.2	7.2	7.2	6.3	10.1	11.7	12.4	13.0
8-CSK *Type-I* **Criterion II**	5.7	10.6	10.7	10.7	10.7	4.6	9.0	10.0	10.7	10.9
8-CSK *Type-II* **Criterion I**	6.8	7.2	7.2	7.2	7.2	5.6	10.0	11.0	11.7	11.9
8-CSK *Type-II* **Criterion II**	5.9	9.7	11.0	11.2	11.2	4.8	8.4	9.6	10.3	10.6
16-CSK *Type-I* **Criterion I**	6.5	8.0	8.0	8.0	8.0	5.0	9.0	10.5	11.1	11.5
16-CSK *Type-I* **Criterion II**	5.7	10.1	13.0	13.0	13.0	4.6	8.9	10.8	11.5	11.8
16-CSK *Type-II* **Criterion I**	9.6	10.0	10.0	10.0	10.0	6.2	10.8	12.7	13.4	13.7
16-CSK *Type-II* **Criterion II**	8.3	12.5	13.5	14.4	14.4	7.3	11.6	12.8	13.5	13.6

the performance limitations of the two-stage system. Furthermore, the BER results closely match the EXIT-chart-based performance predictions shown in Fig. 7. However, compared to the results shown in Fig. 6(c), the BER performance was not improved but actually degraded for all the systems relying on Criterion II. On the other hand, with the aid of the URC precoder, Criterion I attained a substantial iteration gain in the low SNR range, which is an explicit benefit of its capability of efficiently spreading the *extrinsic* information. Again, for the other color constellation schemes of Fig. 2, the BER performance would exhibit the same trend, which will not be detailed here.

Upon comparing Figs. 6(c) and 8, we observe that the BER performance of the two-stage system relying on Criterion II is similar to that of the three-stage system using Criterion I in the BER range of 10^{-4} to 10^{-5}. The overall coding gain summary of our coded M-CSK system has been listed in Table IV, where we define the overall coding gain as the SNR improvement at the BER level of 10^{-6} after each iteration. Hence, we can opt for the most appropriate system according to the specific BER versus complexity requirements.

D. Transmission Distance Improvement

Based on the BER results of Fig. 6(c), let us now investigate how the different signal labeling designs would affect the attainable transmission distance. To demonstrate this, let us assume a simple point-to-point transmission. Hence, the channel matrix $\mathbf{H}$ still remains a diagonal matrix, with each entry given by the channel gain $H(0)$ formulated as [4]

$$H(0) = \frac{(m+1)A_r}{2\pi D^2} \cos^m(\phi)\cos(\psi)T_s(\psi)g(\psi) \tag{15}$$

where A_r represents the physical area of the PD, which is exemplified by a value of 1 cm^2 according to [4]. Furthermore, $m = -\log_2[\cos(\phi_{1/2})]$ is the order of Lambertian emission, which is given by the semi-angle at half-illuminance of the LED used, such as for example $\phi_{1/2} = 60^\circ$, and D denotes the physical distance between the transmitter and receiver, and ϕ and ψ represent the angle of irradiance and incidence, respectively. For simplicity, we let $\phi = \psi = 0^\circ$. Still referring to (15), $T_s(\psi) = 1$ is the gain of the optical filter, and we assume having a field of view of $\psi_c = 60^\circ$ and a refractive index for the lens at a PD, which is $n_{\text{PD}} = 1.5$, as well as an optical concentrator gain of $g(\psi) = n_{\text{PD}}^2/\sin^2(\psi_c) = 3$. Then, upon considering two-stage 8-CSK *Type II* color constellation as an example, according to Section II-B, the received electronic SNR becomes $\gamma_e = (\eta P_{\text{x}})^2/\sigma^2 = [\eta P_{\text{tx}} H(0)]^2/\sigma^2$, where P_{tx} is the transmission power of the LED, whereas η represents the responsivity of the PD assuming idealized lossless reception associated with $\eta = 1$. Furthermore, given that the data rate of 8-CSK is 36 Mb/s [16], according to [4], we have $\sigma^2 = 5.0 \times 10^{-16}$. Finally, if we let $P_{\text{tx}} = 10$ mW and aim for BER $= 10^{-6}$, while assuming that the total average power of the CSK modulation is constant, the achievable transmit distance D can eventually be expressed as

$$D = \sqrt{\frac{A_r P_{\text{tx}} g(\psi)}{\pi\sqrt{\gamma_e \sigma^2}}}. \tag{16}$$

Hence, based on (16), we investigate the beneficial effect of different signal labeling design criteria on the attainable transmit distance D, which is characterized in Fig. 9. Observe that our proposed signal labeling using Criterion II has the best performance, which is capable of increasing the transmit distance while maintaining a BER of 10^{-6}. In practical vehicle-to-vehicle communication and vehicle-to-infrastructure communication, the transmission power is larger than the experimental power that we used here. This implies that, by carefully designing signal labeling according to proper FEC coding and detection scheme, we could realize higher transmission quality in limited range or longer but reliable data transmission. However, as predicted in Fig. 3, due to the limited iteration gain of all other signal labeling strategies, except for the proposed one using Criterion II, the distance improvement attained after two iterations tends to be small, particularly for Criterion I. By contrast, observe in Fig. 9 that for our proposed signal labeling using Criterion II, the improvement between each iteration is a more considerable. This distance improvement is indeed expected for the two-stage system Criterion II because we demonstrated in Fig. 8 that it needs 4-dB lower electronic SNR than its Criterion I counterpart based on the BER versus SNR curves of Fig. 6(c).

IV. CONCLUSION

Efficient signal labeling techniques were designed for both types of CSK color constellations proposed in [16] and [19]–[22]. We provided the EXIT-chart-based performance analysis of both our two-stage and three-stage iterative-detection-aided CSK systems. Commencing from the conventional ML HD, we characterized both the empirical and analytical BER performance of different CSK schemes, adopting the IEEE standard constellation labeling of [16]. We

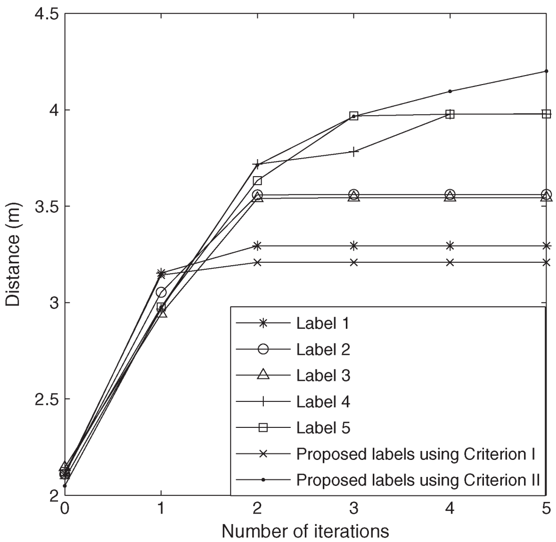

Fig. 9. Achievable transmit distance of a colored LED relying on the two-stage half-rate RSC coded 8-CSK *Type II* system of Fig. 1(b) using the different labeling strategies detailed in Fig. 5, where the LED's transmit optical power is 10 mW, and error tolerance level is BER $= 10^{-6}$. Additionally, the signal labeling using Criterion I is used as a benchmarker.

then demonstrated in Fig. 3 that all the standard M-CSK labeling schemes of Fig. 3(a) and (b) exhibit a limited iteration gain in the context of the joint MAP-based SD-aided iterative receiver of Fig. 1(b). Hence, more beneficial signal labeling schemes were proposed based on the design criterion of (10). The associated numerical BER performances were presented in Fig. 6. We discussed the potential distance and quality improvements of coded CSK in vehicle-related communication and concluded that Criterion II is more beneficial in a two-stage system, whereas Criterion I has the edge in a three-stage system.

REFERENCES

[1] L. Hanzo *et al.*, "Wireless myths, realities, and futures: From 3G/4G to optical and quantum wireless," *Proc. IEEE*, vol. 100, pp. 1853–1888, May 2012.

[2] A. Ghosh *et al.*, "Heterogeneous cellular networks: From theory to practice," *IEEE Commun. Mag.*, vol. 50, no. 6, pp. 54–64, Jun. 2012.

[3] T. S. Rappaport *et al.*, "Millimeter wave mobile communications for 5G cellular: It will work!" *IEEE Access*, vol. 1, pp. 335–349, May 2013.

[4] T. Komine and M. Nakagawa, "Fundamental analysis for visible-light communication system using LED lights," *IEEE Trans. Consum. Electron.*, vol. 50, no. 1, pp. 100–107, Feb. 2004.

[5] S. Rajagopal, R. D. Roberts, and S.-K. Lim, "IEEE 802.15.7 visible light communication: Modulation schemes and dimming support," *IEEE Commun. Mag.*, vol. 50, no. 3, pp. 72–82, Mar. 2012.

[6] J. Grubor, S. Randel, K.-D. Langer, and J. W. Walewski, "Broadband information broadcasting using led-based interior light," *J. Lightw. Technol.*, vol. 26, no. 24, pp. 3883–3892, Dec. 2009.

[7] R. Zhang and L. Hanzo, "Multi-layer modulation for intensity modulated direct-detection optical OFDM," *IEEE/OSA J. Opt. Commun. Netw.*, vol. 5, no. 12, pp. 1402–1412, Dec. 2013.

[8] X. Bao, X. Zhu, T. Song, and Y. Ou, "Protocol design and capacity analysis in hybrid network of visible light communication and OFDMA systems," *IEEE Trans. Veh. Technol.*, vol. 63, no. 4, pp. 1770–1778, May 2014.

[9] J. M. Alattar and J. M. H. Elmirghani, "Optical wireless system employing adaptive collaborative transmitters in an indoor channel," *IEEE Trans. Veh. Technol.*, vol. 59, no. 1, pp. 63–74, Jan. 2010.

[10] A. Ghosh, R. Ratasuk, B. Mondal, N. Mangalvedhe, and T. Thomas, "LTE-advanced: Next-generation wireless broadband technology," *IEEE Wireless Commun.*, vol. 17, no. 3, pp. 1536–1284, Jun. 2010.

[11] V. W. S. Chen, "Free-Space optical communications," *J. Lightw. Technol.*, vol. 24, no. 12, pp. 4750–4762, Dec. 2006.

[12] H. Elgala, R. Mesleh, and H. Haas, "Indoor broadcasting via white LEDs and OFDM," *IEEE Trans. Consum. Electron.*, vol. 55, no. 3, pp. 1127–1134, Aug. 2009.

[13] T. Komine, J. H. Lee, S. Haruyama, and M. Nakagawa, "Adaptive equalization system for visible light wireless communication utilizing multiple white LED light equipment," *IEEE Trans. Wireless Commun.*, vol. 8, no. 6, pp. 2892–2900, Jun. 2009.

[14] R. Mesleh, H. Elgala, and H. Haas, "LED nonlinearity mitigation techniques in optical wireless OFDM communications systems," *IEEE/OSA J. Opt. Commun. Netw.*, vol. 4, no. 11, pp. 865–875, Nov. 2012.

[15] Y. A. Alqudah and M. Kavehrad, "Optimum order of angel diversity with equal-gain combining receivers for broad-band indoor optical wireless communications," *IEEE Trans. Veh. Technol.*, vol. 53, no. 1, pp. 94–105, Jan. 2004.

[16] *IEEE Comput. Soc., IEEE Standard for Local and Metropolitan Area Networks—Part 15.7: Short-Range Wireless Optical Communication Using Visible Light*, Sep. 6, 2011.

[17] *IEEE Comput. Soc. Project: IEEE P802.15 Working Group for Wireless Personal Area Networks (WPANs)*, Jul. 2011.

[18] S. He, G. Ren, Z. Zhong, and Y. Zhao, "M-ary variable period modulation for indoor visible light communication system," *IEEE Commun. Lett.*, vol. 17, no. 7, pp. 1325–1328, Jul. 2013.

[19] R. J. Drost and B. M. Sadler, "Constellation design for color-shift keying using billiards algorithms," in *Proc. IEEE GLOBECOM Workshop*, Miami, FL, USA, Dec.6–10, 2010, pp. 980–984.

[20] R. J. Drost and B. M. Sadler, "Constellation design for channel precompensation in multi-wavelength visible light communications," *IEEE Trans. Commun.*, vol. 62, no. 6, pp. 1995–2005, Jun. 2014.

[21] E. Monterio and S. Hranilovic, "Constellation design for color-shift keying using interior point methods," in *Proc. IEEE GLOBECOM Workshop*, Anaheim, CA, USA, Dec. 3–7, 2012, pp. 1224–1228.

[22] E. Monterio and S. Hranilovic, "Design and implementation of color-shift keying for visible light communications," *J. Lightw. Technol.*, vol. 32, no. 10, pp. 2053–2060, May 2014.

[23] R. Singh, T. O'Farrell, and J. David, "An enhanced color shift keying modulation scheme for high speed wireless visible light communications," *J. Lightw. Technol.*, vol. 32, no. 14, pp. 2582–2592, Jul. 2014.

[24] J. M. Luna-Rivera *et al.*, "Multiuser CSK scheme for indoor visible light communications," *Opt. Exp.*, vol. 22, no. 20, pp. 24256–24257, Oct. 2014.

[25] A. Ashikhmin, G. Kramer, and S. ten Brink, "Extrinsic information transfer functions: Model and erasure channel properties," *IEEE Trans. Inf. Theory*, vol. 50, no. 11, pp. 2657–2673, Nov. 2004.

[26] S. ten Brink, "Convergence behavior of iteratively decoded parallel concatenated codes," *IEEE Trans. Commun.*, vol. 49, no. 10, pp. 1727–1737, Oct. 2001.

[27] M. El-Hajjar and L. Hanzo, "EXIT charts for system design and analysis," *IEEE Commun. Survey Tuts.*, vol. 16, no. 1, pp. 1–27, May 2013.

[28] X. Qi, S. Zhou, M. Zhao, and J. Wang, "Design of constellation labeling maps for iteratively demapped modulation schemes based on the assumption of hard-decision virtual channels," *Proc. Inst. Elect. Eng.–Commun.*, vol. 152, no. 6, pp. 1139–1148, Dec. 2005.

[29] "Commission Internationale de lEclairage Proc." CIE, Vienna, Austria, 1931.

[30] M. K. Simon and M.-S. Alouini, *Digital Communication over Fading Channel*. Hoboken, NJ, USA: Wiley, 2005.

[31] L. Hanzo, O. Alamri, M. El-Hajjar, and N. Wu, *Near Capacity Multi-functional MIMO Systems*. Hoboken, NJ, USA:Wiley, 2009.

[32] X. Wang and H. V. Poor, "Iterative (Turbo) soft interference cancellation and decoding for coded CDMA," *IEEE Trans. Commun.*, vol. 47, no. 7, pp. 1046–1061, Jul. 1999.

[33] A. Chindapol and J. A. Ritcey, "Design, analysis, and performance evaluation for BICM-ID with square QAM constellations in rayleigh fading channels," *IEEE J. Sel. Areas Commun.*, vol. 19, no. 5, pp. 944–957, May 2001.

[34] X. Li, A. Chindapol, and J. A. Ritcey, "Bit-interleaved coded modulation with iterative decoding and 8PSK signaling," *IEEE Trans. Commun.*, vol. 50, no. 8, pp. 1250–1257, Aug. 2002.

[35] N. H. Tran and H. H. Nguyen, "Signal mapping of 8-ary constellations for bit interleaved coded modulation with iterative decoding," *IEEE Trans. Broadcast.*, vol. 52, no. 1, pp. 92–99, Mar. 2006.

Junyi Jiang received the B.Eng. degree in communication engineering from Heilongjiang Institute of Science and Technology, Harbin, China, in 2009 and the M.Sc. degree with distinction in wireless communication from the University of Southampton, Southampton, U.K., in 2010. He is currently working toward the Ph.D. degree with the Wireless Group, School of Electronics and Computer Science, University of Southampton.

His research interests include indoor visible-light communications, free-space optical communications, and iterative detection.

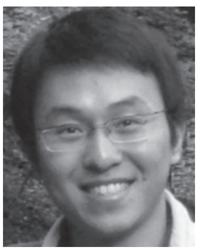

Rong Zhang (M'09) received the B.Sc. degree from Southeast University, Nanjing, China, in 2003 and the Ph.D. degree from the University of Southampton, Southampton, U.K., in 2009.

From August 2003 to July 2004, he was an Engineer with China Telecom. From January 2006 to May 2009, he was a Research Assistant with the Mobile Virtual Center of Excellence, U.K. From August 2009 to July 2012, he was a Postdoctoral Researcher with the University of Southampton. From August 2012 to January 2013, he was a System Algorithms Specialist for Huawei Sweden. Since February 2013, he has been appointed as a Lecturer with the Wireless Group, School of Electronics and Computer Science, University of Southampton. He is also a Visiting Researcher under the Worldwide University Network. He is the author of more than 40 papers published in prestigious journals (e.g., IEEE and The Optical Society) and major conference proceedings.

Dr. Zhang serves as a Reviewer for IEEE TRANSACTIONS/JOURNALS and as a Technical Program Committee Member/Invited Session Chair of major conferences. He received joint funding from the Mobile Virtual Center of Excellence, U.K. and the Engineering and Physical Sciences Research Council, U.K.

Lajos Hanzo (M'91–SM'92–F'04) received the Master's degree in electronics, the Ph.D. degree, and the Doctor Honoris Causa degree from the Technical University of Budapest, Budapest, Hungary, in 1976, 1983, and 2009, respectively.

During his 38-year career in telecommunications, he has held various research and academic posts in Hungary, Germany, and U.K. Since 1986, he has been with the School of Electronics and Computer Science, University of Southampton, Southampton, U.K., where he is currently the Chair in telecommunications. He is also a Chaired Professor with Tsinghua University, Beijing, China. He has successfully supervised about 100 Ph.D. students, coauthored 20 John Wiley/IEEE Press books on mobile radio communications totalling in excess of 10 000 pages, and published more than 1400 research entries on IEEE Xplore. Currently, he is directing a 100-strong academic research team, working on a range of research projects in the field of wireless multimedia communications sponsored by industry, the Engineering and Physical Sciences Research Council (EPSRC) U.K., the European Research Council through an Advanced Fellow Grant, and the Royal Society through the Wolfson Research Merit Award. He is an enthusiastic supporter of industrial and academic liaison, and he offers a wide range of industrial courses.

Dr. Hanzo has acted both as Technical Program Committee and General Chair of IEEE conferences, presented keynote lectures, and received a number of distinctions. He was a Governor of the IEEE Vehicular Technology Society from 2012 to 2014. He was the Editor-in-Chief of the IEEE Press. His research is funded by the European Research Council's Senior Research Fellow Grant. He is a Fellow of the Royal Academy of Engineering, Institution of Engineering and Technology, and European Association for Signal Processing.

AUTHOR QUERY

NO QUERY.